Title	Study on flow instability for feasibility of a thin liquid film first wall
Author(s)	Okino, Fumito; Kasada, Ryuta; Konishi, Satoshi
Citation	Fusion Engineering and Design (2014), 89(7-8): 1054-1058
Issue Date	2014-02
URL	http://hdl.handle.net/2433/187929
Right	© 2014 Elsevier B.V.
Type	Journal Article
Textversion	author

Study on flow instability for feasibility of a thin liquid film first wall

Fumito Okino[a], Ryuta Kasada[b], Satoshi Konishi[b]

[a]Kyoto University Graduate School of Energy Science, Gokasho Uji, Kyoto
[b]Kyoto University Institute of Advanced Energy, Gokasho Uji, Kyoto

This study proposes a probability of the evaporated gas that agitates a growing instability wave in a thin liquid film first wall. The liquid first wall was considered to be in vacuum and the effect of the ambient gas was neglected but the evaporated gas by the high energy fluxes is a probable cause of unstable wave agitation. The criterion is approximately expressed by the density ratio (Q_2) and the Weber number (We) as $Q_2 \times We^{0.5} \approx 5 \times 10^{-4}$. Performed indirect experimental supported this criterion. For a case study of liquid Pb-17Li film with a velocity of 10 m/s, the evaporated gas pressure must be below 6.2×10^3 Pa to maintain stable conditions. By recent study, this pressure is generated at 1600K temperature and it is believed to be attainable by the energy fluxes on the first wall. This result is so far not confirmed so the full verification by experimental is to be performed.

Keywords: Liquid film, first wall, instability, ambient gas, Pb-17Li, evaporation

1. Introduction

Previous studies of the thin liquid metal film first wall for fusion engineering can be categorized into two groups. Here the liquid first wall includes the liquid film which flows along the internal wall and the straight free fall of the fusion core or ICF chamber. Both work as a first barrier from the high energy fluxes. The first group is primarily focused on the behavior and damage of the liquid film due to high-energy fluxes [1-8]. In these studies, fluctuations in the liquid film thickness are not considered. The second group of studies focuses on the fluctuation and stability of the liquid film, which is the approach taken in this study. Ying, Abdou [9] studied the criteria for fluid stability using the Reynolds number and the Weber number. Reperan, Yoda et al. [10, 11] observed flat flow stability and detachment, and Kondo, Suzuki et al. [12, 13] observed wave height distributions. Kunugi, Kawara et al. studied the design concept of stable free flow [14, 15]. Many other such studies have been conducted.

Thus far, the liquid metal film has been treated as in a vacuum condition, and the effect of an ambient gas was not considered as an instability factor. However, the authors predicted that the evaporated gas on the liquid metal film by high energy flux is a probable source of the ambient gas even in the vacuum chamber. To verify this effect, the critical condition of ambient gas for maintaining stable condition in a falling liquid film is analyzed. Then the effect of the evaporated gas is considered.

The liquid metal first wall is generally considered to flow along the large radius internal wall surface. But as far as the interaction between the liquid surface and the ambient gas, the free fall liquid film and the flow along the large radius wall do not behave differently, because both are in the surface tension domain. So the simple free fall model is assumed for the analysis and experimental.

2. Theoretical Analysis

2.1 Instability analysis

The growing wave formation was first analyzed by Squire [16] and Fraser [17] via the temporal single component method. The method was later expanded to a full complex analysis by Luca [18], Lin [19] and other forerunners. The instability wave on a liquid film is known to grow not only temporarily but also spatially. But as far as treating the large time asymptotic behavior and high We number condition, only the convective instability is known to remain, which is the disturbance propagates downstream with the group velocity U_g and grow temporarily and also spatially [20]. Due to the temporal non-dimensionalized factor $U_0/H_0 >> 1$ in this study, the convective instability is approximated as the temporal instability flows down with original flow velocity U_0. Hereafter, the normal temporal mode solution presented by Lin [20] is used for the analysis which is considered as an appropriate level method for this first step feasibility study.

2.2 Fluctuation wave equation

The small surface fluctuation of temporal instability is expressed as

$$f' = f_0\, e^{i(kx - \omega t)} \tag{1},$$

where k, ω and f_0 are the non-dimensional wave number (real) of the x-axis, the complex angular frequency and an arbitrary constant (real), respectively. In this article, x-axis dimension is nondimensionalized by H_0 as $x = x^*/H_0$, where x, x^* and H_0 is the x-axis dimensional length, nondimensionalized length and half film thickness, respectively. At the free fall boundary condition, ω is known to have two independent, sinusoidal and varicose, wave mode solutions as expressed below [20].

$$\omega_s(k) = \omega_s^r \pm B_s^{1/2} = \frac{k \tanh(k)}{Q_2 + \tanh(k)} \pm$$

$$\left[\left(\frac{1}{Q_2 + \tanh(k)} \right)^2 \left\{ \frac{k^3}{We}(Q_2 + \tanh(k)) - k^2 Q_2 \tanh(k) \right\} \right]^{1/2} \quad (2)$$

$$\omega_v(k) = \omega_v^r \pm B_v^{1/2} = \frac{k \coth(k)}{Q_2 + \coth(k)} \pm$$

$$\left[\left(\frac{1}{Q_2 + \coth(k)} \right)^2 \left\{ \frac{k^3}{We}(Q_2 + \coth(k)) - k^2 Q_2 \coth(k) \right\} \right]^{1/2} \quad (3)$$

where superscript r means real number, subscript s and v means sinusoidal and varicose, respectively. Q_2 and We (Weber number) are defined as

$$Q_2 = \frac{\rho_2}{\rho_1}; \quad We = \frac{\rho_1 U_1^2 H_0}{\sigma} \quad (4)$$

where ρ_2 and ρ_1 are the density of the ambient gas and the flowing liquid, respectively. U_1, H_0 and σ are the flow velocity, half of the liquid film thickness and the liquid surface tension, respectively. Bv and Bs are the discriminant of each equation. For a negative discriminant value, the wave grows exponentially.

2.3 Fastest growing wave number

Each discriminant of above equation (2) (3) is known to have a negative minimum. This minimum corresponds to the square of the fastest growing temporal amplitude. For $Q2 \ll 1$ and $k < 1$, the above discriminants can be simplified as

$$B_s(k) \approx \frac{k^2}{We} - k Q_2 \quad (5)$$

$$B_v(k) \approx \frac{k^4}{We} - k^3 Q_2 \quad (6).$$

By taking the derivative with respect to k, each independent fastest wave number can be described by equation(7), with a simple ratio of 2:3.

$$k_s^m : k_v^m = \frac{2Q_2 We}{4} : \frac{3Q_2 We}{4} = 2 : 3 \quad (7)$$

where superscript m means the fastest wave number.

As shown in Fig. 1, the two fastest growing waves merge and evolve to a single amplified wave. This situation is unfavorable for maintaining a stable liquid film thickness. The merged wave number k_{sp} can be described using each fastest wave number, as(9)

$$f_{sp}(x) = \sin(k_s^m x) + \sin(k_v^m x + \alpha)$$

$$= 2 \sin \left\{ \frac{(k_s^m + k_v^m)}{2} x + \frac{\alpha}{2} \right\} \cos \left\{ \boxed{\frac{(k_s^m - k_v^m)}{2}} x - \frac{\alpha}{2} \right\} \quad (8)$$

$$k_{sp} = \left| 2 \frac{(k_s^m - k_v^m)}{2} \right| = | k_s^m - k_v^m | \quad (9)$$
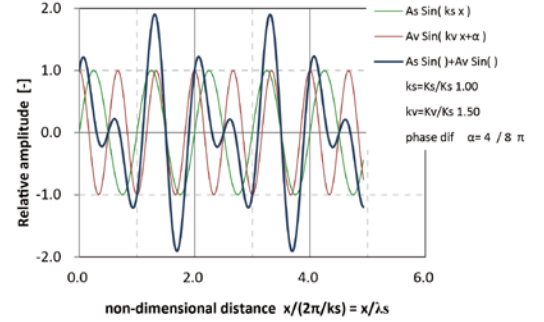
where, α is an arbitrary phase difference.

Fig. 1. Diagram of two superimposed waves.

Two independent waves (thin straight line) and a merged wave (bold line) are shown. The wave number ratio is 2:3, and the phase difference α is $1/2\ \pi$.

2.4 Critical condition of wave growth

The above two independent waves do not evolve unless each discriminant, Bv and Bs, has a negative minimum. Then, the density ratio Q_2 required to maintain both discriminants as positive is found from a numerical comparison of equations (2) and (3) for a given We number. The result is shown in Fig. 2. Beyond the triangles (upper right) is the wave growth zone. The critical condition is approximately expressed as

$$Q_2 \cdot We^{0.5} \approx 5 \times 10^{-4} \quad (10)$$

Below this line, the liquid film flow is stable, and the surface wave does not grow. For the case study of a Pb-17Li flow at a velocity of 10 m/s, the evaporated gas pressure must be below 6.2×10^3 Pa.
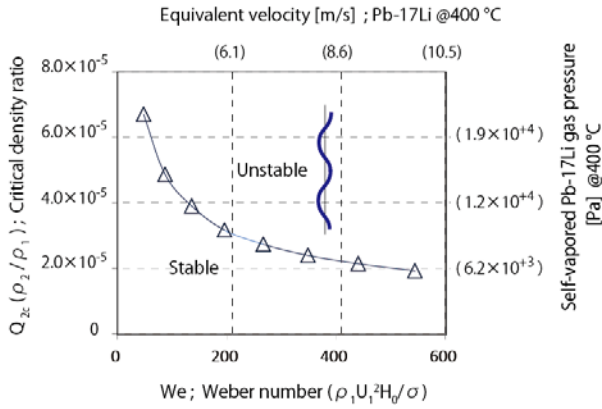
Fig. 2. Plots of the critical density ratio as a function of Weber number.

Below the triangles (lower left) lies the stable zone. This line is approximately expressed as $Q_2 \times We^{0.5} \approx 5\times10^{-4}$. As a reference, the velocity of liquid Pb-17Li and the evaporated gas pressure are given on a second scale.

3. Experimental

3.1 Verification method

To verify the deduced critical condition, described as Fig. 2, the experimental verification with the density ratio parameter and the We number parameter is mandatory. Though in this study, due to the limitation of experimental setup, the deduced fastest growing unstable wave number ksp Eq. (9) with the We number parameter was experimentally verified. The wave behavior of a liquid film is characterized by the non-dimensional Reynolds number, Froude number and Weber number. As shown in Table 1, liquid Pb-17Li and normal water exhibit similar wave motion behavior under this experimental condition. Thus, rather than liquid Pb-17Li, normal water was used for an experimental.

3.2 Experimental setup

An overall view of the experimental setup is shown in Fig. 3. Water liquid film was emitted from a 35-mm-wide slit with a 0.5-mm gap and then flowed down along two 350-mm-long knife-edge guides. Many previous studies about the thin liquid film first wall, the film thickness was assumed between 0.5 mm and 1 mm [9, 11, 22, 23]. To obtain enough gap and flow-width, gap and flow-length ratio, in this experimental, 0.5 mm was assumed. The initial velocity was calculated from the reading of the flow meter and the slit configuration. The initial flow velocity ranged from 4 m/s to 9 m/s. Below 3 m/s, breakup of the film occasionally occurred near the slit. For velocities higher than 9 m/s, breakup of the film also occurred.

Fig. 3. Overall view of the experimental setup.

Liquid film is generated by a 35-mm-wide slit at the top with a 0.5-mm gap and then flows along the knife-edge between two guide-posts. The flow velocity ranged between 3 m/s and 9 m/s.

3.3 Observed wavelength

The surface fluctuation of the falling liquid film was observed by a digital camera as depicted in Fig. 4. To visualize the crest and the bottom of the wave as a difference in brightness, lighting was projected from lower 60 degree angle. In case of a wave-length of 1 mm, the critical detectable amplitude is 0.09 mm, which is appropriate level for this experimental. Difference of the amplitude, though it is not linear proportional, can be recognized as a difference of the shadow region which is described as a bold line length in Fig. 4.
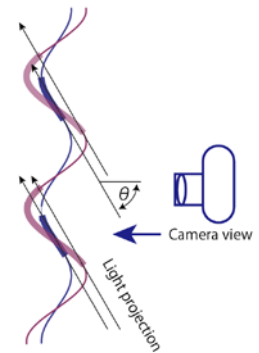

Fig. 4. A schematic of the light projection angle and the shadow region by the crest and bottom of wave front.

The shadow region is described by the bold line. The shadow region increases as the wave amplitude increases, though it is not proportional. By θ 60 degree projection, the wavelength 1mm with amplitude of 0.09 mm can be recognized.

The observed image example is shown in Fig. 5-a. The digitized result of the image is also shown in Fig. 5-b. The central flow region was analyzed, and both edge waves were eliminated. The surface density profile, which corresponds to the surface brightness, was normalized by 256 bits, as shown in Fig. 5-b. The largest amplitude wave component of the surface fluctuation was analyzed using the FFT method. The region of interest (ROI) was 180 mm long $\times$ 5 mm wide, and three different ROIs per surface were analyzed. The result for an 8-m/s flow surface is shown in Fig. 6.
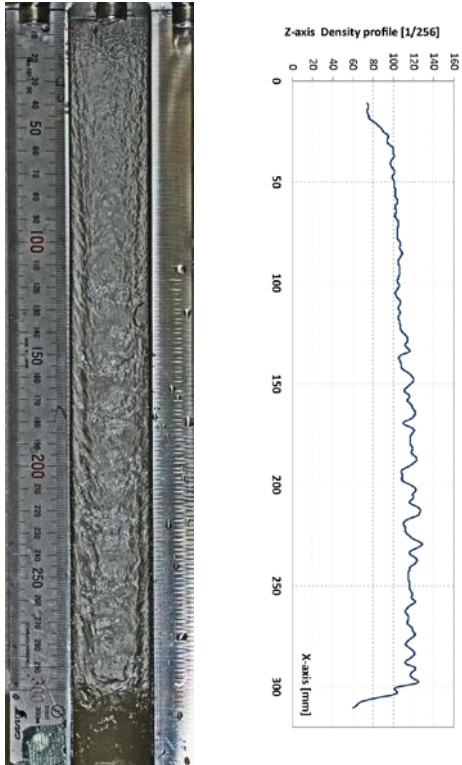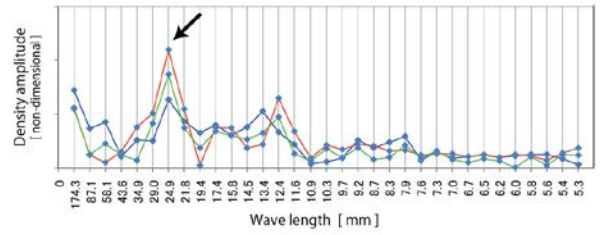

Fig. 6. FFT analysis results of the density profile of Fig. 5-b.

The horizontal axis is the wave-length of N-th Fourier series component. The vertical axis is the amplitude of each component of normalized density profile. Three results from different ROI on a Fig. 5-a are plotted in a same chart. The wave-length of 24.9 mm reveals the largest amplitude component of the surface fluctuation on a Fig. 5-a.

4. Results and Discussion

4.1 Results

The observed largest amplitude wave number and analytically predicted wave number are both plotted in Fig. 7. The predicted wave numbers showed good agreement with the observed results for We $\leq$ 230. At We = 290, the results deviated from the theory. A shift to another wave mode was predicted. These results confirm the initial stage of the wave growth process. Thus the unstable wave growth criterion on Fig. 2, which is deduced from the same instability theory, is indirectly supported.
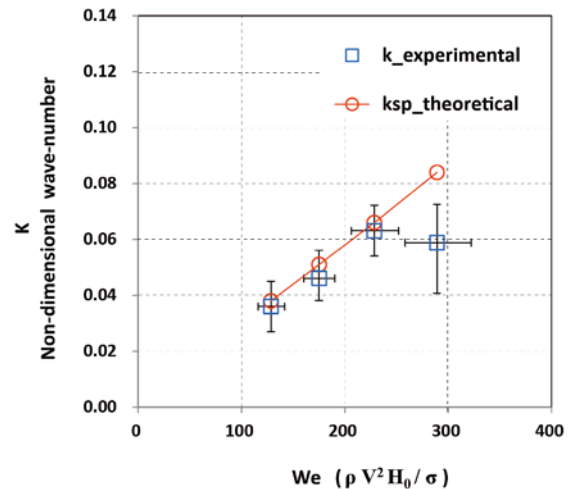

Fig. 5-a (Left). Photograph image of the observed water film surface fluctuation.

U_1 = 8 m/s, Q_2 = 1.2×10^{-3}, We = $2.3 \times 10^{+2}$, $Q_2 We^{0.5}$ = 1.8×10^{-2}. The vertical axis is the flow direction (x-axis). (Camera; Nikon D-7000 with Speed-light SB-600 lighting period 1/24000 sec.)

Fig. 5-b (Right). Density profile of the water film surface. The left image was processed.

The horizontal axis is the 2^8 bit normalized density profile, corresponding to the darker and lighter regions of the right-hand image. Fluctuations of less than 1 mm were eliminated.

Fig. 7. The observed largest amplitude wave number k (□) as a function of Weber number (We). The theoretically predicted largest amplitude wave number ksp (○) is also plotted.

At We < 230, the observed results agree with the theory. At We = 290, the observed results deviate from the theory. A shift to another wave mode is predicted to occur between 230 and 290, due to the decreasing growth time constant.

4.2 Discussions

4.2.1 Temporal and spatial instability

The attained results revealed the typical characteristics of the convective instability wave fluctuation. However, only by this digital picture result, it is not enough to determine. The observation of a wave propagation by the continuous motion pictures is mandatory. For further detail study, it should be considered.

4.2.2 Evaporated gas pressure

The predicted gas pressure at the critical condition of 10 m /s Pb-17Li liquid film flow, which is the typical velocity of the thin liquid metal film first wall concepts [9, 11, 22, 23], is approximately 6.2×10^3 Pa. According to the recent study about the evaporation of liquid Pb-17Li [21], this pressure is attained at approximately 1600 K temperature and it is presumed as a probable value by previous studies [1, 5, 6, 7, 24].

3. Conclusion

In this work, unstable wave growth of a thin liquid film first wall with ambient gas, particularly by an evaporated gas under vacuum condition, was examined.

By analytical study, the Weber number (We) and the density ratio (Q_2) of liquid and ambient gas are the primary factors of unstable wave growth. The deduced criteria is $Q_2 \cdot We^{0.5} \approx 5 \times 10^{-4}$. Performed experimental is considered to support this.

For a case study of liquid Pb-17Li thin film of 10 m / s, the evaporated gas pressure at a critical condition is generated at 1600K temperature. It is predicted to be attainable under the high energy fluxes. This result might require some reconsideration for the feasibility of liquid first wall concept. But this criteria is not verified, so further examinations particularly by the full covered experimental are expected to be performed.

Acknowledgments

References

[1] M. A. Abdou and APEX Team, Exploring novel high power density concepts for attractive fusion systems, Fusion Eng. Des. 45 (1999) 145-167

[2] M. A. Abdou and APEX Team, On the exploration of innovative concepts for fusion chamber technology, Fusion Eng. des. 54 (2001) 181-247

[3] M. Uebeyli, Damage study for various materials at the first wall of a magnetic fusion reactor using protective liquid wall, Fusion Eng. Des. **83** (2008) 1508-511

[4] R.E. Nygre, T.D. Rognlien, M.E. Rensink, S.S. Smolentsev, M.Z. Youssef, M.E. Sawan et. al, A fusion reactor design with a liquid first wall and divertor, Fusion Eng. des. **72** (2004) 181-221

[5] N. B. Morley, Compressible response of thin liquid film/porous substrate first walls in IFE reactors, Fusion Eng. Des. **42** (1998) 563-568

[6] A. R. Raffray, D. Haynes and F. Najmabadi, IFE chamber walls: requirements, design options, and synergy with MFE plasma facing components, J. Nuc. Mat. **313-316** (2003) 23-31

[7] H. Furukawa, Y. Kozaki, K. Yamamoto, T. Johzaki and K. Mima, Simulation on interactions of X-ray and charged particles with first wall for IFE reactor, Fusion Eng. Des. **73** (2005) 95-103

[8] R. W. Moir, Liquid wall inertial fusion energy power plants, Fusion Eng. Des. **32-33** (1996) 93-104

[9] A. Ying and M. Abdou, Scaling Criteria for IFE liquid wall protection scheme simulation, Fusion Eng. Des. **42** (1998) 555-561

[10] J. J. R. Reperant, S. G. Durbin, M. Yoda, S. I. Abdel-Khalik and D. L. Sadowski, Studies of turbulent liquid sheets for protecting IFE reactor chamber first walls, Fusion Eng. Des. **63-64** (2002) 627-633

[11] M. Yoda, S. I. Abdel-Khalik and ARIES-IFE Team, An Investigation of the Fluid Dynamics Aspects of Thin Liquid Film Protection Schemes for Inertial Fusion Energy Reactor Chambers, Fusion Sci. Tech. **46** (2004) 451-469

[12] H. Kondo, T. Kanemura, H. Sugiura, N. Yamaoka, M. Ida, H. Nalamura et al., Development of measurement technique for surface waves on high-speed liquid lithium jet for IFMIF target, Fusion Eng. Des. **85** (2010) 1102-1105

[13] S. Y. Suzuki, H. Sugiura, E. Hoashi, H. Kondo, T. Kanemura, N. Yamaoka et al., Overview : Free surface measurement with renewed nozzle of Osaka Li loop, Fusion Eng. Des. **86** (2011) 2577-2580

[14] T. Kunugi , T. Nakai, Z. Kawara, T. Norimatsu and Y. Kozaki, Investigation of cascade-type falling liquid-film along first wall of laser-fusion reactor, Fusion Eng. Des. **83** (2008) 1888-1892

[15] Z. Kawara, K. Yamamoto, T. Kumugi and T. Norimatsu, Investigation of liquid-film formation along first wall of laser-fusion reactor, Fusion Eng. Des. **85** (2010) 2181-2186

[16] H. B. Squire, Investigation of the instability of a moving liquid film, Brit. J. Appl. Phys. **4** (1953), 167-169

[17] R. P. Fraser, P. Eisenklam, N. Dombrowski, and D. Hasson, Drop Formation from rapidly Moving Liquid Sheets, A. I. Ch. E. Journal Vol. **8** No. 5 (1962) 672-680.

[18] L.D. Luca and M. Costa, Instability of a spatially developing liquid sheet, J. Fluid Mech. **331** (1997) 127-144

[19] S. P. Lin, Z. W. Lian and B. J. Creighton, Absolute and convective instability of a liquid sheet, J. Fluid Mech. **220** (1990) 673-689

[20] S. P. Lin, Breakup of liquid sheets and Jets, Cambridge University Press 2003, ISBN 0-521-80694-1

[21] M. Kondo and Y. Nakajima, Boiling points of liquid breeders for fusion blankets, Fusion Eng. Des. 88 (2013) 2556-2559.

[22] R.W. Moir, HYLIFE-II Inertial Confinement Fusion Reactor Design, UCRL-JC-103816 Rev.1 (1991)

[23] H. Kondo, T. Furukawa, Y. Hirakawa, K. Nakamura, M. Ida,

K. Watanabe et al., IFMIF/EVEDA lithium test loop: design and fabrication technology of target assembly as a key component, Nucl. Fusion 51 (2011) 123008 (12p)

[24] M.Z. Youssef, N. Morley, and A. El-Azab, X-Ray surface and volumetric heat deposition and tritium breeding issues in liquid-protected FW in high power density devices, 13th Topical Meeting on the Technology of Fusion Poer, June 7-11, 1998, Nashville, Tennessee.

Table 1. Non-dimensional parameters of water (H_2O) and Pb-17Li.
(The characteristic length is assumed as the thickness of the film of this experimental.)

	Density	Viscosity	Surface tension	Temperature	Characteristic velocity	Characteristic length	Reynolds number	Froude number	Weber number
	ρ	μ	σ	T	U	L	Re	Fr	We
	Kg / m^3	N s /m^2	N / m	°C	M / s	m	UL/ν	U^2/gL	$\rho U^2 L/\sigma$
H_2O	1.0×10^3	1.0×10^{-3}	0.7×10^{-1}	20	3	5.0×10^{-4}	1.5×10^3	1.8×10^3	6.4×10^1
Pb-17Li	9.7×10^3	1.5×10^{-3}	4.5×10^{-1}	400	3	5.0×10^{-4}	9.7×10^3	1.8×10^3	9.7×10^1